

Stretch-induced changes in arrhythmogenesis and excitability in experimentally based heart cell models

TARA L. RIEMER, ERIC A. SOBIE, AND LESLIE TUNG

Department of Biomedical Engineering, Johns Hopkins University, Baltimore, Maryland 21205

Riemer, Tara L., Eric A. Sobie, and Leslie Tung. Stretch-induced changes in arrhythmogenesis and excitability in experimentally based heart cell models. *Am. J. Physiol.* 275 (*Heart Circ. Physiol.* 44): H431–H442, 1998.—Mechano-electric coupling in the heart is well documented and has been suggested as a cause of arrhythmia. One hypothesized mechanism for the stretch sensitivity of cardiac muscle is the presence of stretch-activated channels (SACs). This study uses modeling to explore the influence of SACs on cardiac resting potential, excitation threshold, and action potential in the context of arrhythmia. We added a putative SAC, modeled as a linear, time-independent conductance with reversal potential of -20 or -50 mV, to guinea pig and frog ventricular membrane models. Increased stretch conductance led to resting potential depolarization, a decreased excitation threshold, altered action potential duration, and, under certain conditions, early afterdepolarizations. We conclude that stretch increases cellular excitability, making the heart prone to ectopic activity. Regional effects of stretch on action potential duration can vary and are influenced by factors such as the SAC reversal potential, ionic conditions, and baseline currents, all of which may lead to an increased dispersion of refractoriness throughout the heart and therefore an increased risk of arrhythmia.

mechanoelectric coupling; electrical stimulation; cardiac myocytes; stretch-activated channels; mathematical model

THE EXISTENCE of cardiac mechanoelectric coupling (the influence of mechanical events on the electrical state of the heart) is well established (for reviews, see Refs. 13 and 27). Clinically, an increased prevalence of arrhythmia is reported for hearts that have been mechanically compromised by congestive heart failure (12, 34) or for hearts that have been exposed to pressure overload through hypertension (46) or aortic valve disease (9). In vitro studies have shown that sudden incidents of cardiac tissue stretch can result in extrasystoles or the formation of arrhythmia (14, 19). It has been hypothesized that stretch-activated channels (SACs) contribute to cellular membrane potential changes and therefore are the underlying cellular substrate for mechanoelectric coupling and stretch-induced arrhythmias (15, 47).

Stretch of cardiac tissue, cells, or cell membranes has been repeatedly observed to alter resting potential (V_{rest}) and action potentials. Stretch-induced changes in V_{rest} , although varied in magnitude, generally act to depolarize the transmembrane potential (V_m). Rapid, pulsatile increases in muscle length or ventricular volume produce transient depolarizations of V_{rest} that can lead to extrasystoles (15, 47). Contrary to this consistent pattern of changes in V_{rest} , stretch-induced action potential changes are highly variable (13, 27).

Because a change in action potential duration (APD) through the consequent heterogeneity of refractoriness (18), dispersion of repolarization (24), formation of early afterdepolarizations (EADs) (36), or wavelength shortening (38) may be a critical factor involved in arrhythmia formation, the variability in action potential shape and duration is important to characterize. An accelerated repolarization caused by tissue or cellular stretch, indicated by a reduction in APD as measured near final repolarization [i.e., APD at 90% repolarization (APD_{90})], has been observed in whole rabbit heart (37), frog ventricle (26), guinea pig papillary muscle (32), frog ventricular myocytes (50), guinea pig ventricular myocytes (54), and in vivo human studies (48). Paradoxically, other studies show shortening of early repolarization (decreased APD at 20% repolarization) followed by a prolonged plateau and delay in final repolarization (increased APD_{90}), resulting in an overall lengthening of the action potential in canine heart (14), rabbit heart (55), and frog ventricle (25).

Because these experimental studies were conducted on various animal preparations by different investigators, it is difficult to reconcile the apparently conflicting effects of stretch on the action potential. It is unclear whether a single mechanism causes all of these stretch effects or whether different mechanisms act in the various preparations and conditions. Modeling of cellular membrane currents and membrane potentials is one approach to address this question because it allows the methodical variation of any number of parameters to permit a thorough and efficient examination.

In this investigation, we explore the relationship between stretch and possible cellular substrates for arrhythmia, such as increased dispersion of repolarization or the formation of EADs. To explore the potential role of SACs in excitability and arrhythmogenesis, we combined a putative SAC model with the Luo-Rudy membrane model for guinea pig ventricle (GPV model) (28, 58). We also formulated and implemented the SAC model into a new biophysical membrane model for frog ventricle (FV model) because the only quantitative report of stretch effects on cellular excitability is with field excitation of frog ventricular cells (50). Moreover, implementation of the FV model permitted us to explore the potential role of the sarcoplasmic reticulum (SR), which has little function in the frog compared with the mammal (10, 31). The two models illustrate that stretch increases cellular excitability and dispersion of both repolarization and refractoriness—all potentially arrhythmogenic factors.

A preliminary version of this study was presented in abstract form (40).

METHODS

Guinea Pig Ventricular Membrane Model

We implemented the mammalian membrane model of Luo and Rudy (28, 58) for the guinea pig ventricle (GPV model), a formulation based on whole cell and single-channel experimental data. To account for stretch sensitivity, a putative SAC was added to the membrane model. Both single-channel (6, 21, 41) and whole cell (21, 44) current recordings have associated a linear current-voltage relation with SACs. These currents have been shown to be carried by cations (6, 21, 41) and to be generally time independent (21, 44). Reported single-channel reversal potentials are -15 (44), -27 (6), -70 and -2 (21), and -35 to -70 (41) mV. Whole cell reversal potentials have been measured to be -15 (44) and -16 (21) mV.

Thus the stretch channel current (I_s) was assumed to be linear and time independent with variable conductance (g_s) and reversal potential (E_s) with representative values of -50 and -20 mV

$$I_s = g_s(V_m - E_s) \quad (1)$$

For potentials increasingly negative to E_s , the channel contributes an increasing inward current that acts to depolarize V_m .

Standard model conditions. Ionic conditions for the GPV model were (in mM) 140 $[Na]_o$, 5.4 $[K]_o$, and 1.8 $[Ca]_o$ (extracellular Na, K, and Ca concentration, respectively), and temperature was 37°C . At steady-state resting conditions, V_{rest} was -86.5 mV, and intracellular concentrations were (in mM) 18 $[Na]_i$, 145 $[K]_i$, and 1.784×10^{-4} $[Ca]_i$. Membrane conductances were normalized to membrane capacitance and expressed in microsiemens per microfarad. Standard capacitive membrane area (1.534×10^{-4} cm^2), cell volume (38×10^{-6} μl), and cellular subvolumes were used (28).

Frog Ventricular Membrane Model

To explore the potential role of SR in stretch responses and to compare excitation threshold (ET) results with experimental data, we also formulated and implemented a new membrane model for the frog ventricle (FV model) as described in the APPENDIX. To account for stretch sensitivity, the membrane model was modified by the addition of a linear, time-independent SAC as in Eq. 1.

Field excitation framework. It is essential to use an appropriate model to determine ET when comparing modeling results to experimental studies that apply field stimuli (50). Therefore, the membrane models were implemented in an 11-patch field excitation framework to determine cellular excitation under conditions of simulated field stimulation. The details of this framework are presented in the APPENDIX.

Standard model conditions. Ionic conditions for the FV model were (in mM) 110 $[Na]_o$, 3.0 $[K]_o$, 1.0 $[Ca]_o$, and 2.5 $[Mg]_i$ and temperature of 22°C . At steady-state resting conditions, V_{rest} was -85.5 mV, and intracellular concentrations were (in mM) 10 $[Na]_i$, 90 $[K]_i$, and 1.099×10^{-4} $[Ca]_i$. Model conductances were expressed in microsiemens for a cell with a capacitance of 0.1 nF and a volume of 2.5×10^{-6} μl . Membrane conductances were normalized to membrane capacitance and expressed in microsiemens per microfarad.

Validation of FV model. Experimental data were obtained using whole cell voltage and current clamp of single frog ventricular myocytes, isolated as previously described (30). The bath Ringer solution contained (in mM) 110 NaCl, 3 KCl, 1.0 CaCl_2 , 10 glucose, and 10 HEPES, pH 7.25. Pipette

solution consisted of (in mM) 40 KCl, 70 K-glutamate, 10 HEPES, and 10 EGTA, pH 7.18. Experiments were conducted at room temperature (19 – 23°C) using a commercial patch-clamp unit (Dagan 3900 Integrating Patch Clamp, Dagan, Minneapolis, MN). Action potentials were generated by a 10-ms current pulse; voltage-clamp pulses were applied from a holding potential of -85.5 mV. Parameters for the ionic currents of the FV model were adjusted until a close fit of the model to the data was obtained.

Simulations

Simulations were initiated with a zero-stretch conductance using standard model conditions unless otherwise indicated. To determine V_{rest} under stretch conditions, g_s was set to the test value and the membrane potential was allowed to settle to its new value over a period of 250 ms. To initiate action potentials, monophasic, rectangular electrical waveforms of 5-ms duration were applied to the field excitation model for cells initially at steady-state V_{rest} . For each value of g_s tested, V_{rest} was allowed to settle for a period of 150 ms before application of the electrical stimulus. To stretch trigger action potentials, the simulation was initiated with $g_s = 0$ and the membrane potential at rest; after 100 ms, g_s was stepped to the test value for a specified duration and then returned to zero.

Action potentials were simulated for a wide range of values for g_s . Using the FV model, we varied g_s from 0 to 300 $\mu\text{S}/\mu\text{F}$ for an E_s of -20 and -50 mV. With the GPV model, g_s was varied from 0 to 100 $\mu\text{S}/\mu\text{F}$ for the same E_s , -20 and -50 mV.

ET was defined as the minimum half-cell-length potential (HCLP) for which excitation occurred and differs from the transmembrane potential at which regenerative activity occurred, i.e., the "takeoff potential." The HCLP is the potential difference generated by the applied field over a distance equal to one-half of the cell length. An action potential was defined to occur when the membrane potential exceeded 0 mV within 100 ms after the onset of the stimulus.

APD₉₀ was used as a measure of the duration of the action potential and was calculated by determining the time elapsed from the action potential upstroke to the point of 90% repolarization from the maximum overshoot. The upstroke was defined as the instant of maximum rate of rise in membrane potential.

The membrane response for a given stimulus waveform was computed using a second-order Runge-Kutta-Fehlberg algorithm with variable step size no greater than 10 μs (Advanced Computer Simulation Language, Mitchell and Gauthier, Concord, MA) running on a computer workstation (Indy/R4400, Silicon Graphics, Mountain View, CA).

RESULTS

Validation of FV Model

Two types of experimental recordings from frog ventricular myocytes using the whole cell variation of the patch-clamp method were obtained for fitting the parameters of the FV model. The first was the ventricular action potential, obtained with a stimulus pulse under current-clamp conditions. The second was the 400-ms isochronal current-voltage relation obtained under voltage clamp. Here, the membrane potential was initially held at rest (-85.5 mV), clamped to the test potential for 400 ms, and then returned to rest. Experimental data were acquired at a sampling rate of 2 kHz, and the

current values were sampled between 398 and 402 ms after the onset of the test potential and averaged. The resulting value was then plotted against the test pulse voltage.

The model-simulated action potentials and 400-ms isochronal current-voltage relations were determined under clamp protocols and extracellular and intracellular ionic conditions identical to those in the experiments and fit iteratively to the experimental recordings by adjusting the delayed rectifier potassium current (I_K), inward rectifier potassium current (I_{K1}), and sodium-potassium pump current (I_{NaK}). All of the remaining currents were constrained according to findings in the literature as described in the APPENDIX. The experimental and model-simulated frog ventricular action potentials are shown in Fig. 1A and compare favorably in height, duration, V_{rest} , and overall shape. The model-generated 400-ms isochronal current-voltage relation shown in Fig. 1B also faithfully reproduces the experimental voltage-clamp findings.

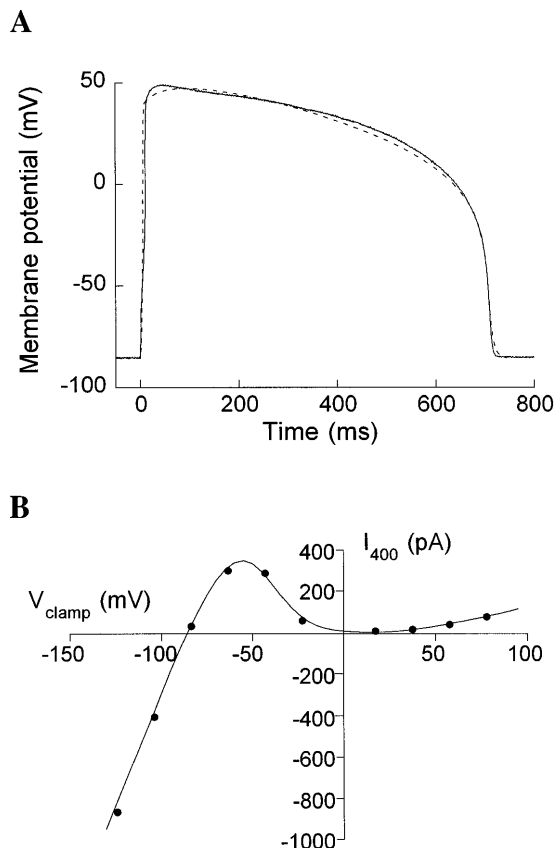


Fig. 1. Comparison of experimental and frog ventricle model (FV model) action potentials and current-voltage (I - V) relations. Standard experimental and model conditions were used. *A*: comparison of experimentally obtained (solid line) and model-simulated (dashed line) frog ventricular action potentials. *B*: isochronal I - V relation measured at 400 ms for FV model compared with experimental data. Ionic membrane current (I_{400}) is plotted on ordinate, and transmembrane potential (V_{clamp}) for actual experimental data (\bullet) and model results (solid line) is plotted on abscissa. Cell capacitance was estimated to be 0.12 nF. Model simulations used a cell capacitance of 0.12 nF, and currents were scaled by 1.2 times from the standard model (capacitance of 0.1 nF).

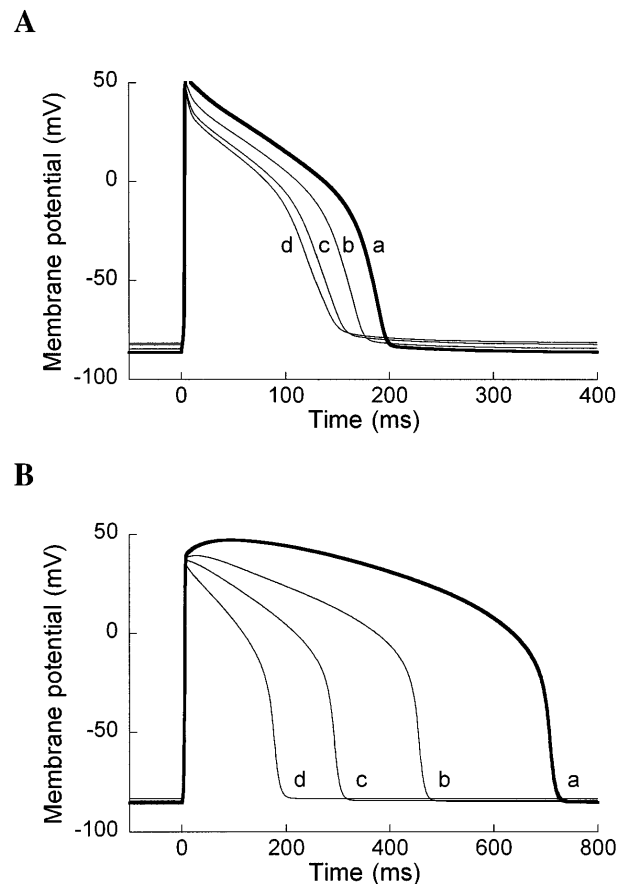


Fig. 2. Comparison of putative action potential changes in guinea pig ventricle (GPV) and FV models with stretch, with reversal potential (E_s) = -50 mV. Standard model conditions were used for all simulations. *A*: GPV model including stretch channel conductance (g_s) of 0 (*a*), 20 (*b*), 40 (*c*), and 50 (*d*) μ S/ μ F. *B*: FV model including g_s of 0 (*a*), 2.5 (*b*), 5 (*c*), and 10 (*d*) μ S/ μ F.

Action Potential Changes

Stretch-mediated changes in APD and action potential shape were explored in both the GPV and FV models by implementing a stretch channel with an E_s of -20 and -50 mV. The stretch channel was activated, and V_{rest} was allowed to stabilize for a period of 150 ms. An electrical field stimulus of a fixed intensity equal to 1.1 times that of the control (unstretched) ET was then applied to trigger an action potential.

Figure 2 shows the results of adding a stretch channel with an E_s of -50 mV in both guinea pig and frog. For guinea pig ventricle, as g_s was increased from 0 to 50 μ S/ μ F, V_{rest} gradually depolarized and APD₉₀ consistently decreased from 193 to 144 ms (Fig. 2A). A similar trend is seen for the frog ventricle. As g_s increased from 0 to 10 μ S/ μ F, V_{rest} depolarized slightly and APD₉₀ decreased to an even larger degree, from 716 to 185 ms (Fig. 2B).

Figure 3 illustrates the analogous case of adding a stretch channel with $E_s = -20$ mV to the GPV and FV models. Here, the effect of the stretch channel on APD was qualitatively different for the two models. For the guinea pig ventricle (Fig. 3A), V_{rest} again depolarized as g_s increased from 0 to 50 μ S/ μ F. However, with in-

creased g_s , APD₉₀ gradually lengthened and final repolarization was delayed; at the same time, the APD measured at plateau levels decreased. These simultaneous events resulted in a characteristic “crossover” of the action potentials during the repolarization phase that was not seen for the case of $E_s = -50$ mV. The action potential plateau lengthening led to the appearance of an EAD ($g_s = 49.6$ $\mu\text{S}/\mu\text{F}$; Fig. 3A, trace c). At a slightly higher level of stretch conductance ($g_s = 50$ $\mu\text{S}/\mu\text{F}$; Fig. 3A, trace d), the EAD triggered a premature action potential. For the frog ventricle (Fig. 3B), V_{rest} depolarized and APD became progressively shorter as g_s increased from 0 to 10 $\mu\text{S}/\mu\text{F}$. This result is similar to that seen for $E_s = -50$ mV.

The ionic basis underlying the EAD and slow action potential upstroke is shown in Fig. 4. During the prolonged plateau (termed the EAD conditional phase; Refs. 22 and 59) preceding the EAD of Fig. 4A, inactivation gates of the L-type calcium current (I_{Ca}) recover while the activation gate closes, permitting reactivation (Fig. 4B). The SR calcium release current (I_{rel}) was not triggered during EAD formation. Therefore, the stretch-induced premature action potential seen in the guinea pig is the result of the recovery and subsequent reactivation of I_{Ca} .

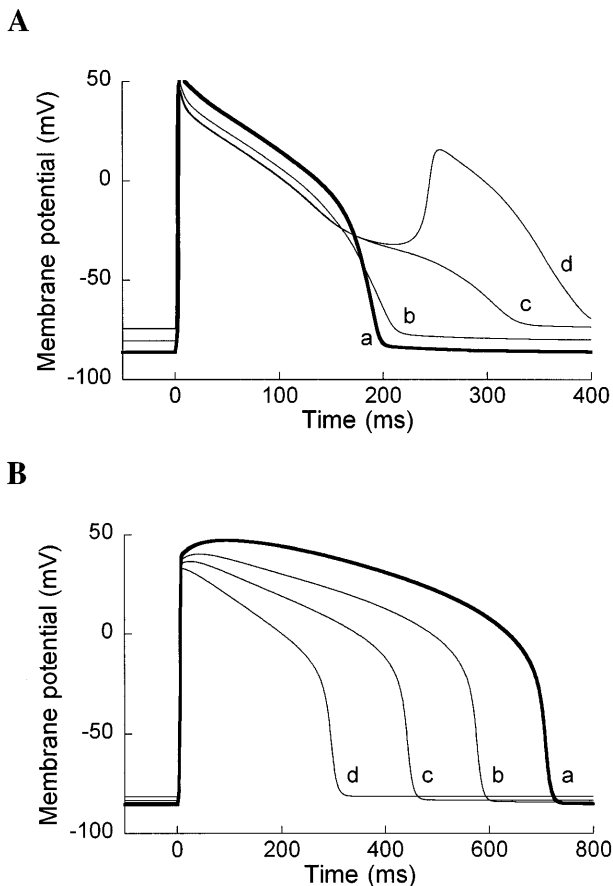


Fig. 3. Comparison of putative action potential changes in GPV and FV models with stretch, with $E_s = -20$ mV. Standard model conditions were used for all simulations. A: GPV model including g_s of 0 (a), 30 (b), 49.6 (c), and 50 (d) $\mu\text{S}/\mu\text{F}$. B: FV model including g_s of 0 (a), 2.5 (b), 5 (c), and 10 (d) $\mu\text{S}/\mu\text{F}$.

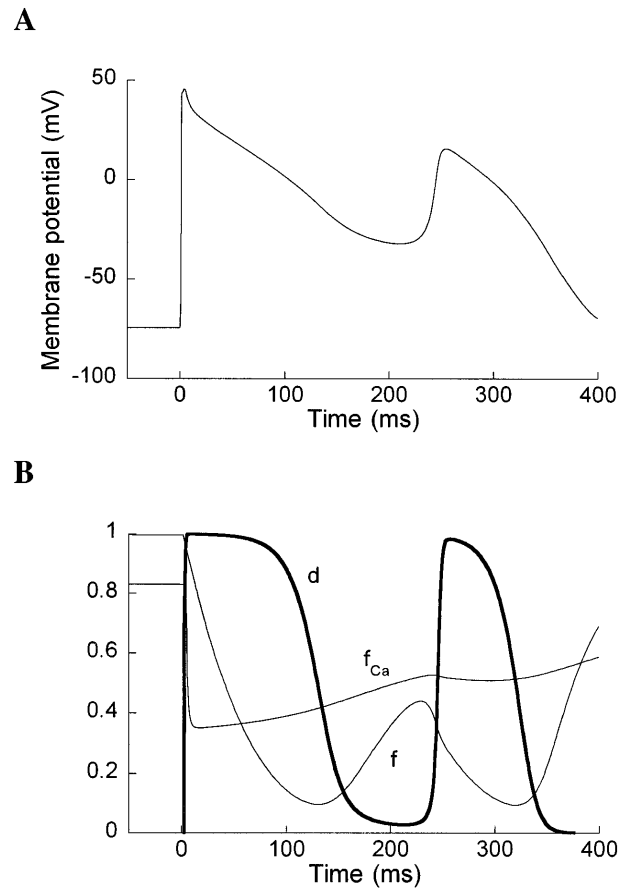


Fig. 4. Kinetic analysis of an early afterdepolarization (EAD) and resulting slow action potential upstroke in GPV model with stretch, with $E_s = -20$ mV. Standard model conditions were used. A: membrane potential for GPV model including g_s of 50 $\mu\text{S}/\mu\text{F}$ (same as trace d of Fig. 3A). B: gating variables for L-type calcium current in A. d , Activation gate; f , inactivation gate; f_{Ca} , calcium-dependent inactivation gate.

Cellular Excitability

To explore the change in excitability of the cell models under stretch, we recorded resting potential (V_{rest}) and ET with increasing g_s . In our simulations using the GPV model, g_s was varied over a range of 0 to 40 $\mu\text{S}/\mu\text{F}$ using an E_s of -20 or -50 mV (Fig. 5). As expected from the results shown in Figs. 2 and 3, V_{rest} depolarized from -86.5 to -78.0 mV over this range for $E_s = -20$ mV and from -86.5 to -82.7 mV for $E_s = -50$ mV. Concurrent with this depolarization of V_{rest} , the cell became more excitable; ET decreased by 23.4% for $E_s = -20$ mV and by 10.4% for $E_s = -50$ mV. Analogous simulations were performed using the FV model. Results similar to those of Fig. 5 were obtained with only minor differences in the curvature of the plots.

A comparison of the effects of g_s on the FV and GPV models is displayed in Table 1. For $E_s = -20$ and -50 mV, the change in V_{rest} (ΔV_{rest}) and the change in ET (ΔET) are given for each model for an increase in g_s from 0 to 40 $\mu\text{S}/\mu\text{F}$. As a measure of comparison, the g_s needed to cause a 12% decrease in ET [$g_s(-12\% \text{ ET})$]

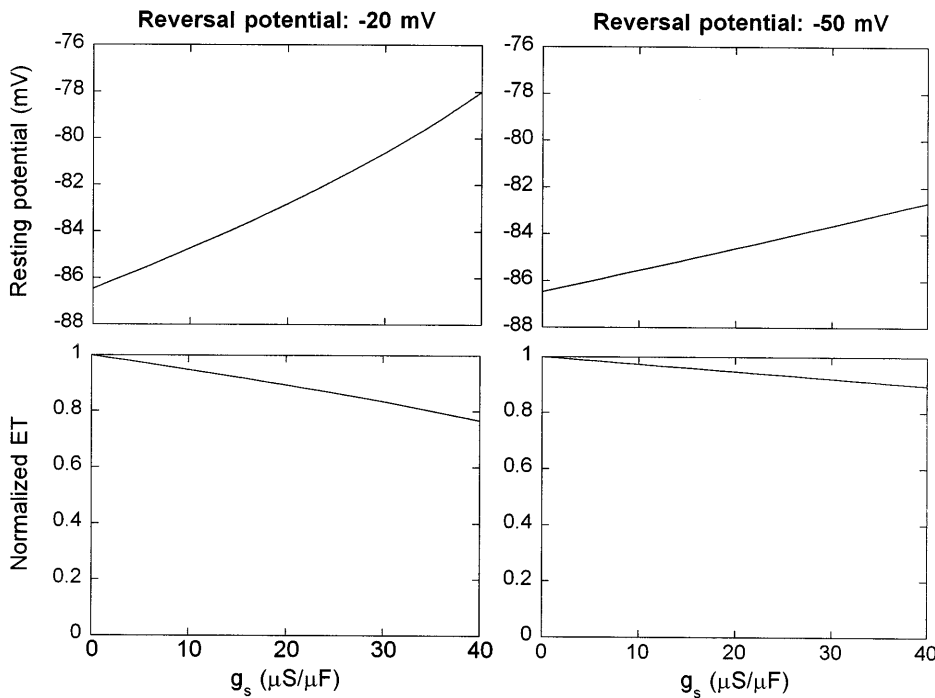


Fig. 5. GPV model predictions for resting potential and excitation threshold (ET) with $E_s = -20$ and -50 mV. *Top*: change in resting potential as a function of g_s , expressed in microsiemens per microfarad. *Bottom*: change in normalized ET as a function of g_s .

was also determined for both models for $E_s = -20$ and -50 mV.

By applying stretch conductances with magnitudes larger than those already discussed, we found that both transient and sustained stretches could directly trigger action potentials in the absence of any electrical stimulus (Fig. 6). Figure 6A shows a guinea pig ventricular action potential triggered by a transient, 30-ms activation of a g_s of $70 \mu\text{S}/\mu\text{F}$ with $E_s = -20$ mV. Figure 6B shows a frog ventricular action potential triggered by a 30-ms, $80 \mu\text{S}/\mu\text{F}$ stretch, also with $E_s = -20$ mV. Similar results were obtained for both guinea pig and frog with $E_s = -50$ mV. A sustained stretch of a slightly lower conductance results in a pacemaker-like activity for guinea pig ventricle. Figure 6C shows the response of the guinea pig ventricular membrane potential to the sustained activation of a g_s of $60 \mu\text{S}/\mu\text{F}$ with $E_s = -20$ mV.

Dispersion of APD

The difference between the changes in APD with stretch obtained with the GPV and FV membrane models at $E_s = -20$ mV (Fig. 3) prompted further investigation. For example, ionic conditions for the FV model were varied to determine whether lengthening of APD_{90} with stretch (behavior never observed under normal ionic conditions for the FV model but seen for

the GPV model in Fig. 3A) could be observed. Indeed, if the magnitude of I_{Ca} were increased, either by simply scaling the current or by increasing $[\text{Ca}]_o$ from 1 to 4 mM, stretch with $E_s = -20$ mV now caused a lengthening of the action potential (Fig. 7A). A similar crossover and increase of APD could also be obtained by a combination of a smaller increase in $[\text{Ca}]_o$ (2 mM) and a decrease in I_{K1} by a factor of 2 (Fig. 6B). However, with either the increase of $[\text{Ca}]_o$ to 2 mM or the decrease of I_{K1} alone, APD shortening (and not lengthening) was observed. Despite significant lengthening of the action potential plateau, no EAD was observed for the FV model under any conditions.

Regional differences in action potential duration in cardiac tissue create a situation of “dispersion of repolarization.” Dispersion of repolarization may be caused by any number of mechanisms, including a gradient in tissue stretch or variance in local extracellular ionic conditions, as suggested by our results. To quantify the potential dispersion of repolarization that might be found in stretched tissue, APD was plotted over a range of g_s for the FV model ($E_s = -20$ mV, Fig. 8). APD_{90} is seen to decrease to less than one-half of its original value with a g_s of $10 \mu\text{S}/\mu\text{F}$ under normal ionic conditions. However, increasing $[\text{Ca}]_o$ to 4 mM or a combination of increasing $[\text{Ca}]_o$ to 2 mM and decreasing

Table 1. Comparison of effects of increased stretch conductance on membrane models

| Model | Δg_s , $\mu\text{S}/\mu\text{F}$ | V_{rest} , mV | $E_s = -20$ mV | | | $E_s = -50$ mV | | |
|----------------------|------------------------------------------|------------------------|-------------------------------|-----------------------|-----------------------------------------------------|-------------------------------|-----------------------|-----------------------------------------------------|
| | | | ΔV_{rest} , mV | ΔET , % | $g_s(-12\% \text{ ET})$, $\mu\text{S}/\mu\text{F}$ | ΔV_{rest} , mV | ΔET , % | $g_s(-12\% \text{ ET})$, $\mu\text{S}/\mu\text{F}$ |
| Guinea pig ventricle | 0→40 | -86.5 | 8.5 | -23.4 | 22.4 | 3.8 | -10.4 | 46.1 |
| Frog ventricle | 0→40 | -85.5 | 14.9 | -37.1 | 11.5 | 7.5 | -18.8 | 23.4 |

E_s , reversal potential of stretch channel; Δg_s , range of stretch conductances tested; V_{rest} , resting potential; ΔET , change in excitation threshold; $g_s(-12\% \text{ ET})$, stretch conductance necessary to produce a 12% decrease of excitation threshold.

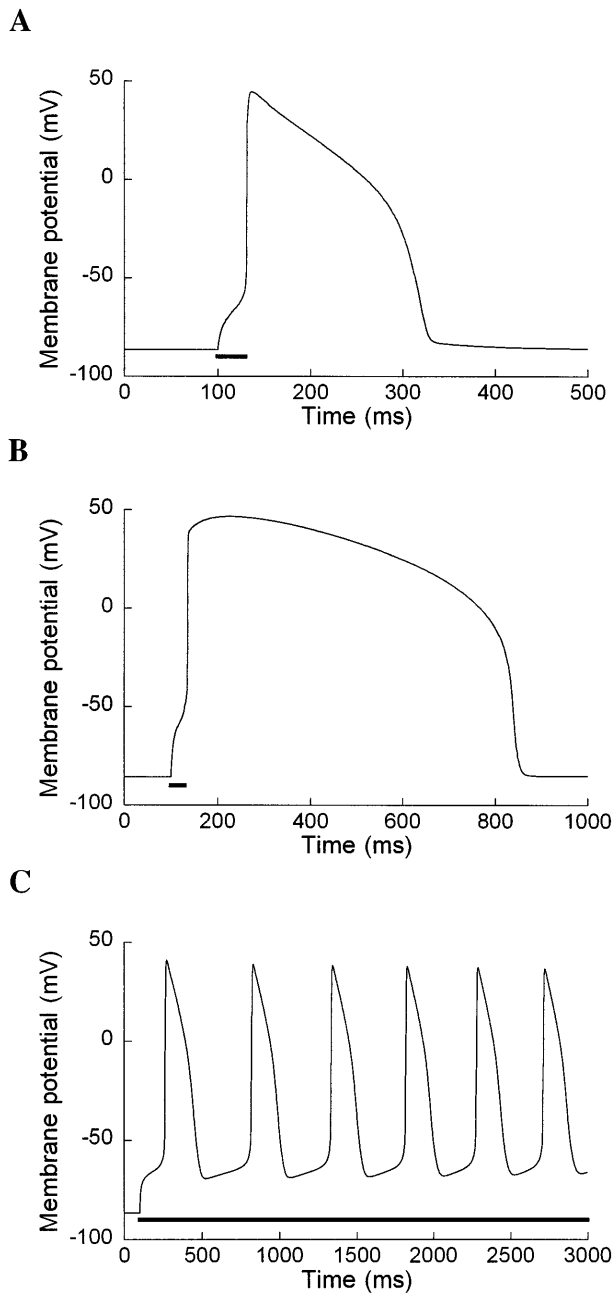


Fig. 6. Stretch-triggered action potentials with $E_s = -20$ mV. A: GPV model including a 30-ms activation of a g_s of $70 \mu\text{S}/\mu\text{F}$. B: FV model including a 30-ms activation of a g_s of $80 \mu\text{S}/\mu\text{F}$. C: GPV model including a sustained activation of a g_s of $60 \mu\text{S}/\mu\text{F}$. Bars indicate duration of g_s activation.

I_{K1} leads to an increase in APD_{90} as g_s increases. Figure 8 illustrates how these APD_{90} changes interact and how given either a gradient in g_s (variation along the abscissa on a single curve) or a regional variation in ionic conditions (variation among curves at a single point on the abscissa), significant dispersion of repolarization can exist in tissue.

DISCUSSION

In this study we implemented two biophysical membrane models, the Luo-Rudy GPV model and a newly

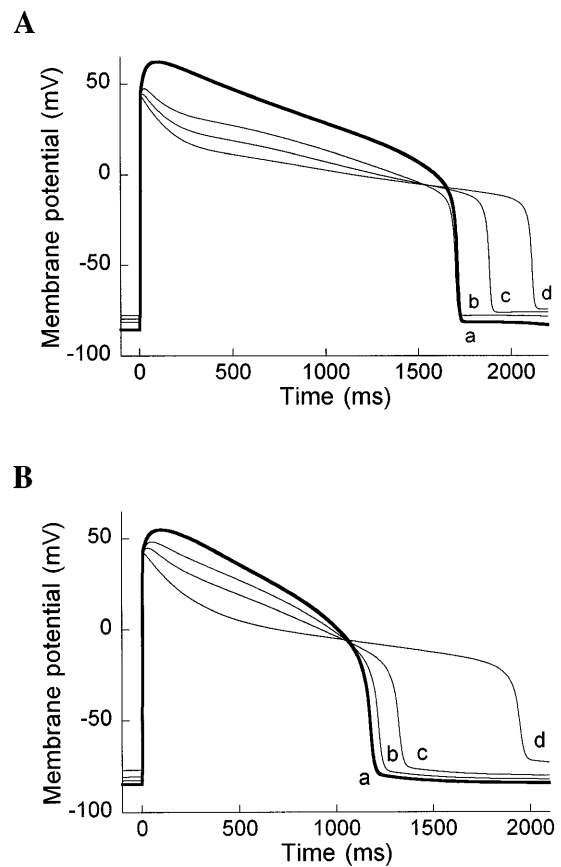


Fig. 7. Comparison of putative action potential changes in FV model with stretch for nonstandard model conditions and $E_s = -20$ mV. A: extracellular Ca concentration ($[\text{Ca}]_o = 4$ mM and g_s of 0 (a), 10 (b), 15 (c), and 20 (d) $\mu\text{S}/\mu\text{F}$. B: $[\text{Ca}]_o = 2$ mM, inward rectifier potassium current (I_{K1}) decreased by a factor of 2, and g_s of 0 (a), 2.5 (b), 5 (c), and 10 (d) $\mu\text{S}/\mu\text{F}$.

formulated FV model, to explore the arrhythmogenic effects of adding a linear, time-independent, stretch-sensitive current. This current consistently caused a depolarization of V_{rest} and a reduction in ET, thus increasing excitability to the point where a mechanical stimulus alone could elicit an extrasystole. APD changes, as measured by APD_{90} , were more variable. The guinea pig action potential shortened with stretch for $E_s = -50$ mV. However, the action potential length-

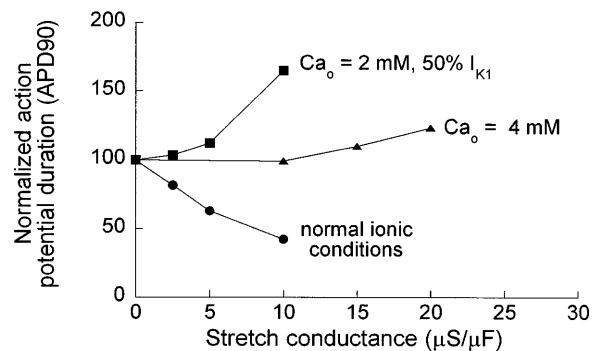


Fig. 8. Action potential duration (APD) variability. APD at 90% repolarization (APD_{90}) is plotted for 3 different cellular conditions for a variety of stretch conductances. ●, Standard conditions; ▲, $[\text{Ca}]_o = 4$ mM; ■, $[\text{Ca}]_o = 2$ mM, I_{K1} decreased by a factor of 2.

ened with stretch for $E_s = -20$ mV, leading to a crossover of the action potentials and formation of EADs. In contrast, the frog action potential consistently shortened with increased stretch for both $E_s = -20$ mV and $E_s = -50$ mV, and neither action potential crossover nor lengthening was seen. Under altered ionic conditions, the frog action potential could lengthen with increased stretch, although EADs were never seen. The highly variable APD response observed in this study suggests that stretch is a possible substrate for arrhythmia in terms of an increased dispersion of repolarization throughout a region of stretched tissue. In addition, the formation of EADs indicates a mechanism for stretch-induced extrasystoles or initiation of reentry.

Effect of Stretch Conductance on ET and V_{rest}

Depolarization of V_{rest} occurs with an increase in the conductance of the stretch channel, a finding that was independent of the membrane model or stretch channel E_s . At times, the depolarization of the membrane potential by the stretch current was sufficient to trigger an action potential independent of any electrical stimulus (Fig. 6), a behavior that corresponds to that seen experimentally in isolated rabbit heart and frog ventricle (15, 25). The ubiquitous V_{rest} depolarization is paralleled by a decrease in ET. Over a range of g_s , a close relationship exists between the extent of depolarization and the percent decrease of ET. The ratio of percent change in ET per millivolt change in V_{rest} was nearly constant and varied only from 2.49 to 2.75 for the range of conductance changes reported (Fig. 5, Table 1).

Such decreases in ET and depolarizations in V_{rest} that occur with applied stretch are consistent with previous findings in cell-based experiments. A recent study of whole cell currents in guinea pig ventricular myocytes has shown the activation of inward stretch-sensitive currents for stretch of 10–20% from resting length (44). Another cell-based study, in which direct mechanical stretch was applied to guinea pig ventricular myocytes, reported a slight depolarization (<4 mV) of V_{rest} with stretch (54).

We, too, have observed small depolarizations of V_{rest} and found $\sim 12\%$ change in ET for a 10% stretch in single frog ventricular myocytes during direct mechanical stretch (Ref. 50; Table 1). These findings, combined with those from the FV model, can be used to estimate the fraction of SACs that are activated by a 10% stretch of a ventricular cell. The values for g_s expected to effect a 12% change in ET are shown in Table 1 and range from 11.5 to 46.1 $\mu\text{S}/\mu\text{F}$. These values for g_s are only a rough estimate, considering the many assumptions that have been made. Nevertheless, the conductance values are quite low when compared with single-channel data. Assuming a single-channel conductance on the order of 100 pS (6, 41), channel density of 0.3/ μm^2 (6, 41), and specific membrane capacitance of 1 $\mu\text{F}/\text{cm}^2$, a g_s of 46.1 $\mu\text{S}/\mu\text{F}$ corresponds to an open probability for the channels on the order of $(46.1 \mu\text{S}/\mu\text{F}) / (100 \text{ pS} \times 0.3/\mu\text{m}^2) \approx 0.015$. Therefore, the stretch conductance activated by a 10% stretch is

$\sim 1.5\%$ of that expected for fully open channels, indicating that only a small fraction of stretch channels need be opened to increase cellular excitability significantly.

Effect of Stretch Conductance on APD

An intriguing result of our simulations is the variety of changes in the morphology of the action potential that can occur with increased stretch. For $E_s = -50$ mV, the action potential consistently shortens with increasing stretch for both membrane models (Fig. 2). However, for $E_s = -20$ mV, the FV model shows APD shortening whereas the GPV model shows APD lengthening as g_s increases (Fig. 3). This action potential lengthening in the GPV model is accompanied by a crossover during repolarization and can ultimately lead to formation of an EAD (Fig. 3A, trace d). Thus our modeling results indicate that differences in E_s (as reported for different subtypes of SACs; Refs. 21 and 41) can modulate stretch-induced changes in APD.

To determine whether other factors can modulate the APD response to stretch, additional simulations were performed in which the relative levels of the ionic currents or ionic concentrations were varied. The possibility that calcium may be a modulator of stretch has been described by Gannier and co-workers (16). Their results show that a stretch-induced increase in intracellular calcium depends on extracellular calcium rather than on intracellular stores and seems to be caused by calcium influx through L-type calcium channels (16), which have been found to be mechanically sensitive (29). We found that in the FV model, the magnitude of I_{Ca} plays a crucial role in the behavior of the action potential with stretch. Our simulation of Fig. 3C was executed with a $[\text{Ca}]_o$ of 1 mM, and action potential shortening was observed. However, if $[\text{Ca}]_o$ were raised to 4 mM, or if the magnitude of I_{Ca} were increased (analogous to upregulation of the channel), action potential lengthening could be induced (Fig. 7A). Augmentation of this current contributes to the creation of a small, negative region of the current-voltage relation during the plateau phase that is not present in the FV model under normal calcium conditions (Fig. 1B). Therefore, a quasi-stable potential is created at approximately -10 mV, leading to the observed lengthening in the action potential.

Taken together, these action potential simulations show that the stretch response of APD may be highly sensitive to a few ionic currents or ionic conditions, leading either to shortening or lengthening of APD from its normal value. Also, activation of a stretch channel does not imply that the point of crossover of action potentials with increasing stretch is necessarily equal to E_s , contrary to the assertions of some previous studies (43). The crossover point may be either positive (Fig. 7) or negative (Fig. 3A) (55) to E_s . Also, a crossover need not always occur (Fig. 3B).

Clinical Implications for Arrhythmogenesis

Both the depolarization in V_{rest} and the decrease in ET seen in this study may be sufficient to produce an

action potential without external electrical stimulation, as was seen in model simulations at high stretch conductances (Fig. 6). Stretch-induced depolarizations have been observed to induce extrasystoles experimentally (3, 19, 25). Pulsatile volume increases in rabbit whole heart preparations induce corresponding V_{rest} depolarizations such that increasing the magnitude of these volume pulses leads to progressively increased depolarizations and eventually to triggered extrasystoles (15). Transient stretch of frog ventricular tissue will also consistently trigger tissue activation that can be detected both mechanically and electrically (11).

The altered durations of the plateau and repolarization phases of the action potential also have proarrhythmic tendencies. An extended plateau can create a conditional phase (22) when the cell is vulnerable to EADs. Once formed, an EAD may trigger a premature upstroke, resulting in an extrasystole. EADs were seen in simulations of the GPV model (Fig. 3A, *trace c*) and were capable of triggering a regenerative upstroke (Fig. 3A, *trace d*).

In contrast, shortening of the action potential does not have any inherently arrhythmogenic effects at the cellular level. However, at the tissue or whole heart level, APD shortening will lead to a reduction in wavelength, known to predispose cardiac tissue to arrhythmia. In addition, regional APD shortening will increase the dispersion of refractoriness and repolarization, also commonly believed to be substrates for arrhythmia formation (18, 24). Such a dispersion of refractoriness would be augmented further if regional lengthening were also to occur in other parts of the heart. Spatially heterogeneous refractoriness and repolarization have been reported in the isolated pig heart when subjected to increased loading by aortic clamping (8), and a significant increase of regional dispersion of repolarization was shown to result from sustained stretch in isolated rabbit hearts (56). This modeling study reinforces these experimental findings and suggests that local variations in stretch levels and ionic conditions may act synergistically, leading to simultaneous action potential shortening and lengthening in different cardiac regions, thereby increasing the dispersion of APD throughout the heart.

The concept that ionic conditions play a role in the modulation of APD under stretch conditions implies that pathological conditions may augment or alter the baseline electrophysiological effects of stretch. During ischemia and reperfusion, membrane currents are modified as a result of altered ionic composition of intracellular and extracellular fluids and the buildup of metabolic byproducts (4). Ischemia leads to an accumulation of extracellular potassium, caused at least partially by an ATP-sensitive potassium channel activated by a decrease in cellular ATP levels (2). There is also considerable evidence for abnormal calcium cycling in heart failure, resulting in altered calcium transients (5). Both ischemia and heart failure, although generally viewed as mechanical disorders, are associated with an increased risk of sudden death by arrhythmia (36, 57). The pathological ionic conditions associated with these

diseases may compound the stretch-induced effects on APD, thereby contributing to an increased dispersion of refractoriness throughout the heart.

In addition to heterogeneity of the magnitude of stretch or of ionic conditions, a heterogeneity of stretch channel types throughout the heart may also increase the dispersion of repolarization. Cells may contain multiple stretch channel subtypes, each having a characteristic E_s and distribution pattern (21, 41). In chick heart cells, for example, two populations of SAC have been identified, having E_s of -70 and -2 mV (21). The effective E_s of the total stretch-induced current will lie between these two E_s and will be determined by the relative conductances contributed by each channel type. If the channels are nonuniformly distributed throughout the heart, so that different channel types dominate regionally, the effective E_s of the stretch-induced current will also vary from region to region. We have shown that in guinea pig cells, stretch can cause either action potential shortening or lengthening depending on the exact value of E_s (Figs. 2A and 3A).

Early Afterdepolarizations

EADs were seen in simulations using the GPV model but not in those using the FV model (Figs. 3, 6). Because SR has a much greater functional role in the mammal compared with the frog (10, 31), we expected that the more complex calcium dynamics of the guinea pig might explain why the GPV model shows a tendency towards EAD formation. However, we found that I_{rel} was zero during the EAD, indicating that some other current must be involved in EAD formation.

In a modeling study by Zeng and Rudy in a guinea pig ventricular cell model (59), the critical factors for drug-induced EAD formation were determined to be a prolonged action potential plateau and reactivation of L-type calcium channels. These two factors are related, because the extended plateau phase provides time for I_{Ca} to recover from inactivation, a necessary precursor to its reactivation. In our experiments using the GPV model, the action potential plateau was lengthened by addition of a stretch current with $E_s = -20$ mV (Fig. 3A). A conditioning phase developed at approximately -30 mV, the same as observed by Zeng and Rudy (59). This potential is sufficiently negative to permit significant ($\sim 40\%$) recovery of inactivation and the subsequent reactivation of I_{Ca} (Fig. 4). In the FV model, a prolonged plateau appeared during stretch only under varied extracellular ionic conditions (Fig. 7). However, this plateau level was 0 to -10 mV, much more positive than that seen for GPV action potentials. At this membrane potential, little recovery from inactivation is possible, and reactivation of the L-type calcium channels does not occur. Because the characteristics of the activation and inactivation gates are nearly identical in the GPV and FV models, the level of the plateau potential may therefore be critical to whether reactivation of I_{Ca} and formation of EADs result from stretch.

There has been some debate as to whether experimental findings of stretch-induced EADs in frog (25) and

mammalian (33) tissue are real or artifactual. Our results suggest that EAD formation, at least in guinea pig, is indeed a real effect of stretch.

Comparison to Previous SAC Modeling Studies

Our model for I_s is similar to the SAC implemented in previous modeling by Sachs (42) and Zabel et al. (55) for guinea pig ventricle using the Oxsoft HEART program. In those simulations, the stretch conductance was explicitly assumed to be a function of sarcomere length, in the form $g_s = \gamma\rho\beta(L)$, where γ is single-channel conductance, ρ is channel density, $\beta(L)$ is a nonlinear length-dependent factor that defines channel open probability, and L is sarcomere length. According to their model, $\beta(L)$ asymptotically approaches zero at short lengths and is 1% activated at a sarcomere length of 1.9 μm , the slack length for guinea pig ventricular myocytes (17). We have made no assumptions regarding the relationship between channel open probability and sarcomere length in our formulation, because this relationship is not currently known.

The previous modeling studies using this SAC formulation illustrated that some stretch-induced action potential and V_{rest} changes reported by experimental studies could be successfully modeled by implementing a linear, time-independent SAC with a negative E_s (42, 55). The current study shows that stretch of cardiac tissue produces more than just a change in the duration of the action potential. The APD change has a significant impact on arrhythmogenicity and excitability of cardiac tissue. Changes in APD, especially when regionally distributed, can become arrhythmogenic through mechanisms such as EADs, wavelength shortening, and increased dispersion of repolarization. Stretch also depolarizes V_{rest} and increases the excitability of individual cardiac cells.

Limitations of Study

The SAC has been assumed to be linear and time-independent, on the basis of findings from numerous experimental studies. Other modeling studies have made the same assumptions with respect to SAC properties (42, 55). However, although experimental studies have confirmed the existence of linear, time-independent SACs in guinea pig (44), direct experimental data have not yet been obtained to show their existence in the frog ventricle. In addition, there may be a slow time-dependent inactivation of SACs, on the order of seconds (21) or minutes (44, 50), that has not been accounted for in this study.

Other ionic effects of stretch have been described for cardiac muscle. First, several of the fundamental time-dependent channels typically found in cardiac cells, including the L-type calcium, delayed rectifier potassium, and ATP-sensitive potassium channels (29, 51, 53), have been shown to be modified by stretch. Second, currents have been identified in frog and guinea pig ventricle that are mechanosensitive but not necessarily stretch sensitive, including the swelling-sensitive chlo-

ride current (39, 52). This current is not activated under isotonic conditions, and therefore is not expected to alter the results of the current study. Third, it is known that the binding of calcium to troponin C is stretch sensitive (7). The effects of stretch on these other mechanisms have not been considered in the current study.

In conclusion, these results confirm experimental observations that stretch of cardiac tissue can be arrhythmogenic. Stretch leads to V_{rest} depolarization and increased cellular excitability. The diversity of APD changes induced by stretch may lead to an increased dispersion of repolarization, a potentially arrhythmogenic situation in cardiac tissue. EADs and premature action potentials can be elicited by a stretch current and may initiate extrasystoles in the whole heart.

APPENDIX: FV MODEL

The FV model simulates the electrophysiological properties of frog ventricular cardiac membrane. The simulation equations for this model are based largely on the model formulated by Rasmusson et al. (35) for the frog atrium (FA model). The FV model assumes a "standard" cell with a capacitance of 10^{-4} μF , the convention used in the FA model. Conductances are expressed in microsiemens, membrane potential in millivolts, and membrane currents in nanoamperes. The diffusion-limited cleft space in the FA model was eliminated. Changes from the FA membrane equations were implemented as necessary to match simulations to whole cell voltage-clamp and action potential data obtained from single frog ventricular myocytes. A putative stretch-activated current was also included in the model.

Model Equations

Sodium current. The kinetic equations used to describe the fast sodium current (I_{Na}) are based on the data of Seyama and Yamaoka (45) for bullfrog ventricular cells. The rate constants were scaled by 5.2 to account for an apparent Q_{10} of 2.5 in these cells (1) and the 18°C temperature difference between experimental (4°C) and model (22°C) conditions. This value of Q_{10} was calculated by comparing the activation time constant data at 4°C (45) with the activation time constant reported for 25°C (1). However, this value of Q_{10} did not account for the difference in the inactivation time constant between these two sets of data (1, 45). To adjust for this discrepancy, the inactivation time constant was increased by a factor of 1.7. The maximum conductance was set to a value of 0.66 μS .

Calcium current. I_{Ca} was the FA calcium current for frog atrial cells scaled by a factor of 2.125 as reported in a current density comparison between frog atrial and ventricular cells (20).

Delayed rectifier potassium current. I_{K} was the FA current scaled by a factor of 0.25 to match the 400-ms isochronal current-voltage relation at positive transmembrane potentials obtained experimentally in frog ventricular cells, as shown in Fig. 1B.

Inward rectifier potassium current. The mathematical formulation for I_{K1} in the FA model had too few free parameters to match our experimental data for frog ventricular cells. Instead, a modified version of the Luo-Rudy I_{K1} current (28) was used, with parameters altered to match the 400-ms isochronal current-voltage relation for transmembrane po-

tentials negative to -20 mV (Fig. 1B). The current was defined by the following equations

$$I_{K1} = g_{K1} (V_m - E_K) \quad (A1)$$

$$g_{K1} = 0.101486 \frac{a_{K1} c_{K1} \sqrt{[K]_o}}{a_{K1} + b_{K1}} \quad (A2)$$

$$a_{K1} = \frac{2.04}{1 + \exp [0.07155(V_m - E_K - 54.215)]} \quad (A3)$$

$$c_{K1} = 1 - \frac{0.9}{1 + \exp [0.11925 (V_m - E_K - 99.215)]} \quad (A4)$$

$$b_{K1} = \frac{\begin{cases} 0.49124 \exp [0.05783(V_m - E_K - 13.524)] \\ + \exp [0.06175(V_m - E_K - 584.31)] \end{cases}}{1 + \exp [-0.5143(V_m - E_K + 14.753)]} \quad (A5)$$

where E_K is the potassium reversal potential.

Background currents. The calcium background current and the sodium background current were identical to those in the FA model.

Stretch-activated current. The putative I_s used in the FV model was assumed to have a time-independent, linear current-voltage relation, with E_s in the range of -50 to -20 mV and a g_s that increased with stretch (Eq. 1).

Pump and exchanger currents. The sodium-calcium exchanger current (I_{NaCa}) and the sarcolemmal calcium pump current were identical to those in the FA model. The sodium-potassium pump current (I_{NaK}) was scaled by a factor of 0.5 from that of the FA model.

Corrections to the FA Model. On the basis of discussions with R. Rasmusson, corrections were made to three published equations of the FA model (35). These equations, including corrections, are also part of the FV model.

Delayed rectifier current

$$r' = \frac{95}{1 + \exp \left(\frac{V_m - E_K - 98}{25} \right)} - 95 \quad (A6)$$

where r' is a variable in the formulation of the maximum conductance of the delayed rectifier current (I_K).

Sodium-potassium pump

$$I_{NaK} = 0.0725 \cdot \left(\frac{[Na]_i}{[Na]_i + 5.46} \right)^3 \left(\frac{[K]_o}{[K]_o + 0.621} \right)^2 \left(\frac{V_m + 150}{V_m + 200} \right) \quad (A7)$$

Sodium-calcium exchanger (incorrect parentheses)

$$I_{NaCa} = 1.5 \times 10^{-6} \cdot \frac{\begin{cases} [Na]_i^3 [Ca]_o \exp (0.0195 V_m) \\ - [Na]_o^3 [Ca]_i \exp (-0.0195 V_m) \end{cases}}{1 + 0.0001([Na]_o^3 [Ca]_i + [Na]_i^3 [Ca]_o)} \quad (A8)$$

Field Excitation

To determine cellular excitation threshold under experimental conditions of field stimulation, the model was modified further in a manner similar to that developed previously (49). Unlike the previous field model in which cells were stimulated by longitudinally oriented fields, here we consider the case of transverse stimulation because this configuration allows a clear separation of membrane channel versus geometric effects, as will become apparent. Assuming a prolate spheroid shape for the cell, the extracellular surface potential

(V_e) resulting from the applied field (E_{oy}) can be determined analytically and is a linear function of distance (y) (23)

$$V_e(y) = A(\epsilon) E_{oy} y \quad (-b \leq y \leq b) \quad (A9)$$

with the form factor (A) being a function of eccentricity (ϵ), defined as $\sqrt{1 - (b^2/a^2)}$, where a and b are the semimajor and semiminor axes, respectively. For simplicity in our model, we have assumed the limiting case of a cylindrical geometry with radius (b) for the cell, in which case $a \rightarrow \infty$, $\epsilon \rightarrow 1$, $A \rightarrow 2$, and V_e assumes the well-known cosine dependence if y is expressed in terms of polar angle (i.e., $y = b \cos \theta$).

The membrane was divided circumferentially into 11 segments over which V_e (varying from $-2E_{oy}b$ to $+2E_{oy}b$) was partitioned into 11 equal ranges. The potential drop over one-half of the cell ($E_{oy}b$), termed the half-cell-length potential (HCLP), was used to define ET. The biophysical properties of each membrane patch were represented by the model equations described by the FV model or the GPV model, and the relative sizes of the membrane patches were calculated as previously described (49). To reduce the simulation times, intracellular and extracellular resistances were omitted, which resulted in a slight but systematic overestimation of ET.

In the interpretation of our simulation results, it is necessary to take into account changes in the cell geometry with stretch. If a constant cell volume is assumed, an increment of $\Delta L/L$ in cell length will decrease cell diameter by $\sqrt{\Delta L/L}$, thereby decreasing the sensitivity of the cell to the extracellular field and raising the stimulus threshold. A 10% longitudinal stretch will result in a 4.65% decrease in cell diameter, resulting in an effective increase in ET by a factor of $100/(100 - 4.65) = 1.05$ from geometric effects alone. In previous experiments from our laboratory, the ET for cross-shock field stimuli in single frog ventricular myocytes was found to decrease on the order of -0.8% per 1% stretch ($n = 10$; Ref. 50). Accounting for the expected geometric changes, the ET for a 10% increase in cell length can be calculated to be $(100 - 8)/1.05 = 87.7\%$ of the prestretch value, i.e., a decrease of $\sim 12\%$. This 12% decrease in ET resulting from a 10% cell stretch is used as a characteristic measure of the stretch effect.

This work was supported by National Institutes of Health Grant R01 HL-50610. T. Riemer was a recipient of a Whitaker Foundation Graduate Fellowship in Biomedical Engineering.

Address for reprint requests: L. Tung, Dept. of Biomedical Engineering, Johns Hopkins Univ., 720 Rutland Ave., Baltimore, MD 21205.

Received 20 November 1997; accepted in final form 20 April 1998.

REFERENCES

1. **Bhatnagar, A., S. K. Srivastava, and G. Szabo.** Oxidative stress alters specific membrane currents in isolated cardiac myocytes. *Circ. Res.* 67: 535-549, 1990.
2. **Billman, G. E.** Role of ATP sensitive potassium channel in extracellular potassium accumulation and cardiac arrhythmias during myocardial ischaemia. *Cardiovasc. Res.* 28: 762-769, 1994.
3. **Brooks, C. M., J. L. Gilbert, and E. E. Suckling.** Excitable cycle of the heart as determined by mechanical stimuli. *Proc. Soc. Exp. Biol. Med.* 117: 634-637, 1964.
4. **Cascio, W. E., T. A. Johnson, and L. S. Gettes.** Electrophysiologic changes in ischemic ventricular myocardium: I. Influence of ionic, metabolic, and energetic changes. *J. Cardiovasc. Electrophysiol.* 6: 1039-1062, 1995.
5. **Colucci, W. S., and E. Braunwald.** Pathophysiology of heart failure. In: *Heart Disease: A Textbook of Cardiovascular Medicine* (5th ed.), edited by E. Braunwald. Philadelphia, PA: Saunders, 1997, p. 394-420.

6. **Craelius, W.** Stretch-activation of rat cardiac myocytes. *Exp. Physiol.* 78: 411–423, 1993.
7. **Crozatier, B.** Stretch-induced modifications of myocardial performance: from ventricular function to cellular and molecular mechanisms. *Cardiovasc. Res.* 32: 25–37, 1996.
8. **Dean, J. W., and M. J. Lab.** Regional changes in ventricular excitability during load manipulation of the in situ pig heart. *J. Physiol. (Lond.)* 429: 387–400, 1990.
9. **Dreifus, L. S.** Arrhythmias in valvular heart disease. *Cardiovasc. Clin.* 23: 65–74, 1993.
10. **Fabiato, A.** Calcium-induced release of calcium from the cardiac sarcoplasmic reticulum. *Am. J. Physiol.* 245 (Cell Physiol. 14): C1–C14, 1983.
11. **Fasciano, R. W., and L. Tung.** Refractory period of the heart probed by uniaxial stretch of cardiac tissue (Abstract). *International Workshop: Mechano-Electrical Feedback and Cardiac Arrhythmias, Trento, Italy, 1997*, p. 39.
12. **Francis, G. S.** Development of arrhythmias in the patient with congestive heart failure: pathophysiology, prevalence and prognosis. *Am. J. Cardiol.* 57: 3B–7B, 1986.
13. **Franz, M. R.** Mechano-electrical feedback in ventricular myocardium. *Cardiovasc. Res.* 32: 15–24, 1996.
14. **Franz, M. R., D. Burkhoff, D. T. Yue, and K. Sagawa.** Mechanically induced action potential changes and arrhythmia in isolated and in situ canine hearts. *Cardiovasc. Res.* 23: 213–223, 1989.
15. **Franz, M. R., R. Cima, D. Wang, D. Proffitt, and R. Kurz.** Electrophysiological effects of myocardial stretch and mechanical determinants of stretch-activated arrhythmias. *Circulation* 86: 968–978, 1992.
16. **Gannier, F., E. White, Garnier, and J. Y. Le Guennec.** A possible mechanism for large stretch-induced increase in $[Ca^{2+}]_i$ in isolated guinea-pig ventricular myocytes. *Cardiovasc. Res.* 32: 158–167, 1996.
17. **Gannier, F., E. White, A. Lacampagne, D. Garnier, and J. Y. Le Guennec.** Streptomycin reverses a large stretch induced increase in $[Ca^{2+}]_i$ in isolated guinea pig ventricular myocytes. *Cardiovasc. Res.* 28: 1193–1198, 1994.
18. **Han, J., and G. K. Moe.** Nonuniform recovery of excitability in ventricular muscle. *Circ. Res.* 14: 44–60, 1964.
19. **Hansen, D. E., C. S. Craig, and L. M. Hondeghem.** Stretch-induced arrhythmias in the isolated canine ventricle. Evidence for the importance of mechano-electrical feedback. *Circulation* 81: 1094–1105, 1990.
20. **Hartzell, H. C., and M. A. Simmons.** Comparison of effects of acetylcholine on calcium and potassium currents in frog atrium and ventricle. *J. Physiol. (Lond.)* 389: 411–422, 1987.
21. **Hu, H., and F. Sachs.** Mechanically activated currents in chick heart cells. *J. Membr. Biol.* 154: 205–216, 1996.
22. **January, C. T., and J. M. Riddle.** Early afterdepolarizations: mechanism of induction and block. A role for L-type Ca^{2+} current. *Circ. Res.* 64: 977–990, 1989.
23. **Klee, M., and R. Plonsey.** Stimulation of spheroidal cells—the role of cell shape. *IEEE Trans. Biomed. Eng.* 23: 347–354, 1976.
24. **Kuo, C. S., K. Munakata, C. P. Reddy, and B. Surawicz.** Characteristics and possible mechanism of ventricular arrhythmia dependent on the dispersion of action potential durations. *Circulation* 67: 1356–1367, 1983.
25. **Lab, M. J.** Mechanically dependent changes in action potentials recorded from the intact frog ventricle. *Circ. Res.* 42: 519–528, 1978.
26. **Lab, M. J.** Transient depolarisation and action potential alterations following mechanical changes in isolated myocardium. *Cardiovasc. Res.* 14: 624–637, 1980.
27. **Lab, M. J.** Mechanoelectric feedback (transduction) in heart: concepts and implications. *Cardiovasc. Res.* 32: 3–14, 1996.
28. **Luo, C. H., and Y. Rudy.** A dynamic model of the cardiac ventricular action potential. I. Simulations of ionic currents and concentration changes. *Circ. Res.* 74: 1071–1096, 1994.
29. **Matsuda, N., N. Hagiwara, M. Shoda, H. Kasanuki, and S. Hosoda.** Enhancement of the L-type Ca^{2+} current by mechanical stimulation in single rabbit cardiac myocytes. *Circ. Res.* 78: 650–659, 1996.
30. **Mitra, R., and M. Morad.** A uniform enzymatic method for dissociation of myocytes from hearts and stomachs of vertebrates. *Am. J. Physiol.* 249 (Heart Circ. Physiol. 18): H1056–H1060, 1985.
31. **Morad, M., and L. Cleemann.** Role of Ca^{2+} channel in development of tension in heart muscle. *J. Mol. Cell. Cardiol.* 19: 527–553, 1987.
32. **Nakagawa, A., M. Arita, T. Shimada, and J. Shirabe.** Effects of mechanical stretch on the membrane potential of guinea pig ventricular muscles. *Jpn. J. Physiol.* 38: 819–838, 1988.
33. **Nazir, S. A., and M. J. Lab.** Mechanoelectric feedback in the atrium of the isolated guinea-pig heart. *Cardiovasc. Res.* 32: 112–119, 1996.
34. **Packer, M.** Sudden unexpected death in patients with congestive heart failure: a second frontier. *Circulation* 72: 681–685, 1985.
35. **Rasmusson, R. L., J. W. Clark, W. R. Giles, K. Robinson, R. B. Clark, E. F. Shibata, and D. L. Campbell.** A mathematical model of electrophysiological activity in a bullfrog atrial cell. *Am. J. Physiol.* 259 (Heart Circ. Physiol. 28): H370–H389, 1990.
36. **Reiter, M. J.** Effects of mechano-electrical feedback: potential arrhythmogenic influence in patients with congestive heart failure. *Cardiovasc. Res.* 32: 44–51, 1996.
37. **Reiter, M. J., D. E. Mann, and G. R. Williams.** Interaction of hypokalemia and ventricular dilatation in isolated rabbit hearts. *Am. J. Physiol.* 265 (Heart Circ. Physiol. 34): H1544–H1550, 1993.
38. **Rensma, P. L., M. A. Allesie, W. J. Lammers, F. I. Bonke, and M. J. Schaliq.** Length of excitation wave and susceptibility to reentrant atrial arrhythmias in normal conscious dogs. *Circ. Res.* 62: 395–410, 1988.
39. **Riemer, T. L., J.-S. Fan, and L. Tung.** Are swelling, pressure, and axial stretch equivalent stimuli for mechano-electrical coupling in heart cells? (Abstract). *International Workshop: Mechano-Electrical Feedback and Cardiac Arrhythmias, Trento, Italy, 1997*, p. 28.
40. **Riemer, T. L., E. A. Sobie, and L. Tung.** Stretch-induced membrane potential changes in single cardiac myocytes can lead to increased dispersion of repolarization (Abstract). *International Workshop: Mechano-Electrical Feedback and Cardiac Arrhythmias, Trento, Italy, 1997*, p. 33.
41. **Ruknudin, A., F. Sachs, and J. O. Bustamante.** Stretch-activated ion channels in tissue-cultured chick heart. *Am. J. Physiol.* 264 (Heart Circ. Physiol. 33): H960–H972, 1993.
42. **Sachs, F.** Modeling mechanical-electrical transduction in the heart. In: *Cell Mechanics and Cellular Engineering*, edited by V. C. Mow, F. Guliak, R. Tran-Son-Tray, and R. M. Hochmuth. New York: Springer, 1994, p. 308–328.
43. **Sachs, F., and G. C. L. Bett.** Cardiac mechanosensitivity and stretch-activated ion channels. *Trends Cardiovasc. Med.* 7: 4–8, 1997.
44. **Sasaki, N., T. Mitsuiye, and A. Noma.** Effects of mechanical stretch on membrane currents of single ventricular myocytes of guinea-pig heart. *Jpn. J. Physiol.* 42: 957–970, 1992.
45. **Seyama, I., and K. Yamaoka.** A study of the electrical characteristics of sodium currents in single ventricular cells of the frog. *J. Physiol. (Lond.)* 401: 257–275, 1988.
46. **Sideris, D. A.** High blood pressure and ventricular arrhythmias. *Eur. Heart J.* 14: 1548–1553, 1993.
47. **Stacy, G. P., Jr., R. L. Jobe, L. K. Taylor, and D. E. Hansen.** Stretch-induced depolarizations as a trigger of arrhythmias in isolated canine left ventricles. *Am. J. Physiol.* 263 (Heart Circ. Physiol. 32): H613–H621, 1992.
48. **Taggart, P., P. Sutton, M. Lab, M. Runnalls, W. O'Brien, and T. Treasure.** Effect of abrupt changes in ventricular loading on repolarization induced by transient aortic occlusion in humans. *Am. J. Physiol.* 263 (Heart Circ. Physiol. 32): H816–H823, 1992.
49. **Tung, L., and J. R. Borderies.** Analysis of electric field stimulation of single cardiac muscle cells. *Biophys. J.* 63: 371–386, 1992.
50. **Tung, L., and S. Zou.** Influence of stretch on excitation threshold of single frog ventricular cells. *Exp. Physiol.* 80: 221–235, 1995.
51. **Van Wagoner, D. R.** Mechanosensitive gating of atrial ATP-sensitive potassium channels. *Circ. Res.* 72: 973–983, 1993.

52. **Vandenberg, J. I., A. Yoshida, K. Kirk, and T. Powell.** Swelling-activated and isoprenaline-activated chloride currents in guinea pig cardiac myocytes have distinct electrophysiology and pharmacology. *J. Gen. Physiol.* 104: 997–1017, 1994.
53. **Wang, Z. R., T. Mitsuiye, and A. Noma.** Cell distension-induced increase of the delayed rectifier K^+ current in guinea pig ventricular myocytes. *Circ. Res.* 78: 466–474, 1996.
54. **White, E., J. Y. Le Guennec, J. M. Nigretto, F. Gannier, J. A. Argibay, and D. Garnier.** The effects of increasing cell length on auxotonic contractions; membrane potential and intracellular calcium transients in single guinea-pig ventricular myocytes. *Exp. Physiol.* 78: 65–78, 1993.
55. **Zabel, M., B. S. Koller, F. Sachs, and M. R. Franz.** Stretch-induced voltage changes in the isolated beating heart: importance of the timing of stretch and implications for stretch-activated ion channels. *Cardiovasc. Res.* 32: 120–130, 1996.
56. **Zabel, M., S. Portnoy, and M. R. Franz.** Effect of sustained load on dispersion of ventricular repolarization and conduction time in the isolated intact rabbit heart. *J. Cardiovasc. Electrophysiol.* 7: 9–16, 1996.
57. **Zehender, M., T. Faber, T. Meinertz, and H. Just.** Clinical evidence for the fatal interaction of ventricular tachyarrhythmias, myocardial ischemia and sudden cardiac death. *Herz* 20: 187–199, 1995.
58. **Zeng, J., K. R. Laurita, D. S. Rosenbaum, and Y. Rudy.** Two components of the delayed rectifier K^+ current in ventricular myocytes of the guinea pig type. Theoretical formulation and their role in repolarization. *Circ. Res.* 77: 140–152, 1995.
59. **Zeng, J., and Y. Rudy.** Early afterdepolarizations in cardiac myocytes: mechanism and rate dependence. *Biophys. J.* 68: 949–964, 1995.

